

## Improved electron probe microanalysis of trace elements in quartz

JOHN J. DONOVAN,<sup>1,\*</sup> HEATHER A. LOWERS,<sup>2</sup> AND BRIAN G. RUSK<sup>3</sup>

<sup>1</sup>CAMCOR, University of Oregon, Eugene, Oregon 97403, U.S.A.

<sup>2</sup>U.S. Geological Survey, MS 973, Denver, Colorado 80225, U.S.A.

<sup>3</sup>School of Earth and Environmental Sciences, James Cook University, Townsville QLD 4811, Australia

### ABSTRACT

Quartz occurs in a wide range of geologic environments throughout the Earth's crust. The concentration and distribution of trace elements in quartz provide information such as temperature and other physical conditions of formation. Trace element analyses with modern electron-probe microanalysis (EPMA) instruments can achieve 99% confidence detection of ~100 ppm with fairly minimal effort for many elements in samples of low to moderate average atomic number such as many common oxides and silicates. However, trace element measurements below 100 ppm in many materials are limited, not only by the precision of the background measurement, but also by the accuracy with which background levels are determined. A new "blank" correction algorithm has been developed and tested on both Cameca and JEOL instruments, which applies a quantitative correction to the emitted X-ray intensities during the iteration of the sample matrix correction based on a zero level (or known trace) abundance calibration standard. This iterated blank correction, when combined with improved background fit models, and an "aggregate" intensity calculation utilizing multiple spectrometer intensities in software for greater geometric efficiency, yields a detection limit of 2 to 3 ppm for Ti and 6 to 7 ppm for Al in quartz at 99% t-test confidence with similar levels for absolute accuracy.

**Keywords:** Electron microprobe, trace elements, quartz, detection limit, accuracy, background artifacts, blank correction, aggregate intensities

### INTRODUCTION

Quartz is the second most abundant mineral in the Earth's crust and is common in plutonic, volcanic, metamorphic, hydrothermal, and sedimentary environments. Because quartz forms in many geologic environments, genetic information derived from quartz geochemical analysis has broad applications in the geosciences. Recent studies have attempted to understand the evolution of various geological processes through trace element analysis of quartz (Wark et al. 2007; Rusk et al. 2008; Müller and Koch-Muller 2009; Larsen et al. 2009; Lehmann et al. 2009; Thomas et al. 2010). These and other studies correlate the physical and chemical conditions of quartz crystallization with the concentration of a variety of trace element constituents, usually Ti and Al at the parts per million levels.

Trace element variations in quartz are typically characterized qualitatively by cathodoluminescent (CL) images (Fig. 1) (Rusk et al. 2006, 2008; Wark and Watson 2006; Allan and Yardley 2007; Landtwing and Pettko 2005; Monecke et al. 2002; Penniston-Dorland 2001). These images often reveal variations in CL texture and intensity that are interpreted as distinct generations of quartz precipitation and dissolution (Rusk and Reed 2002). Careful trace element analyses indicate that fluctuations in CL intensity are primarily due to variations in the concentration of Ti in the range of <2 ppm to several hundred parts per million and Al concentration between a few parts per million and several thousand parts per million. Growth zones and cross-cutting quartz generations are commonly only a few micrometers in

width, and therefore the interpretation of geologic histories based on trace element analysis among various CL features (Mercer and Reed 2010) requires high-resolution analyses (<5  $\mu\text{m}$ ) that are both accurate and precise at concentrations down to a few parts per million (Fig. 2). Although both laser ablation-inductively coupled plasma-mass spectrometry (LA-ICP-MS) and secondary ion mass spectrometry (SIMS) have recently been applied to understanding trace element concentrations in hydrothermal quartz, neither of these techniques can offer the spatial resolution offered by electron-probe microanalysis (EPMA).

Modern EPMA instruments equipped with stable electron guns, low noise gas flow detectors, high-speed counting electronics, and large area analyzing crystals can achieve detection limits for most elements down to 100 ppm or lower with minimal effort. However, artifacts produced in the X-ray continuum due to systematic sample and instrumental effects become increasingly significant issues for accuracy as lower detection limits are sought, particularly at trace concentration levels below several tens of parts per million. Previous studies have achieved detection limits of 10–20 ppm Ti using long counting times (Rusk et al. 2006; Wark and Watson 2006) but systematic accuracy errors resulting from these continuum artifacts limit further improvements in detection limit. In this study, newly developed software techniques permit both significantly improved detection limits and better accuracy for EPMA of many trace elements in quartz. This has been accomplished in three ways; first by implementing improved background models to fit the shape of the background, second by utilizing new quantitative "blank" correction routines for improved background determination accuracy, and third by means of "aggregate" counting methods

\* E-mail: donovan@uoregon.edu

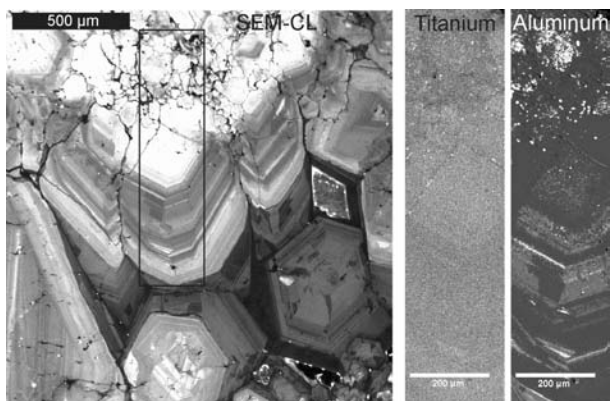


**FIGURE 1.** CL image and Al and Ti trace element WDS maps of vein quartz from the El Salvador porphyry copper deposit, Chile (cf. Rusk et al. 2008), using a JEOL 8900 EPMA. CL image shows early mosaic quartz crystals overgrown by quartz with euhedral growth zones of oscillating CL intensity. CL intensity correlation with Ti concentration is difficult to determine in a  $TiK\alpha$  X-ray map without a proper quantitative background correction.

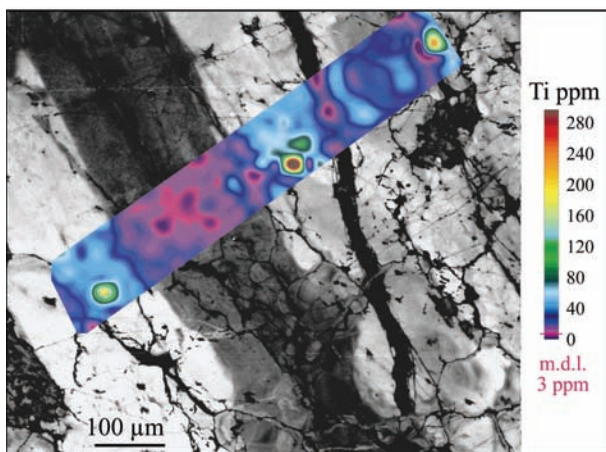


**FIGURE 2.** SEM-CL image of a quartz vein from the porphyry copper deposit in Butte, Montana, overlain with map of quantitative EPMA Ti concentrations (parts per million) contoured based on a grid of 395 microprobe analyses using two spectrometers tuned to  $TiK\alpha$  with the aggregate intensity option for improved detection limits and the quantitative blank correction for improved accuracy. There is excellent agreement between the more intense (white) cathodoluminescent areas of the image and higher Ti abundance although the difference between the two zones is approximately only 20 to 40 ppm.

using multiple spectrometers to improve geometric efficiency for better detection limits. The combination of these software methods yields 99% confidence detection limits of  $\sim 2\text{--}3$  ppm for Ti and  $\sim 6\text{--}7$  ppm for Al, without compromising the high-spatial resolution offered by EPMA.

### BACKGROUND MODELING

There are several causes for systematic accuracy errors in EPMA determinations of trace element concentrations. A common occurrence is the presence of spectral interferences on the

analytical peak of interest by secondary emission lines from other elements also present in the sample matrix [see Donovan et al. (1993) for a full treatment]. Additionally, secondary fluorescence effects from adjacent phases containing major amounts of the trace element of interest can produce spurious detection when characteristic or continuum X-rays emitted from the phase under electron bombardment are able to travel a distance sufficient to excite nearby phases containing that element. For example, measurements of trace Al in quartz are quite susceptible to such errors when Al-rich phases are also present in the sample. This is because the relatively strong  $SiK\alpha$  characteristic emissions produced from electron bombardment of quartz can cause Al atoms in adjacent feldspar grains to fluoresce, resulting in the subsequent emission of  $AlK\alpha$  X-rays, which cannot be spatially resolved even by focusing X-ray spectrometers. Such analytical situations will produce apparent concentrations of 100 to 150 ppm of Al in pure synthetic  $SiO_2$  at distances of tens of micrometers from a mechanically produced  $Al_2O_3$  boundary. Llovet and Galan (2003) and Jercinovic et al. (2008) provide other examples of secondary fluorescence effects on trace element intensities in geological settings. Efforts to produce an analytical expression based software correction for such sources of measurement error, without recourse to time-consuming Monte-Carlo methods, are in progress (Escuder et al. 2010).

However, the primary causes for most systematic accuracy errors in trace element determinations are the result of poorly placed background intensity measurement spectrometer positions and/or improperly selected background fit models for interpolation of the background intensity underneath the peak to determine the net intensity of the emitted characteristic line. For example, if the background measurement position of the element of interest lies near a secondary line of another element, the background intensity will be systematically higher than the true background intensity by a degree proportional to the concentration of the secondary element. To avoid these situations, it is generally necessary to perform high-sensitivity wavelength scans on each side of the analytical peak and choose background positions that are free from interferences at the required sensitivity levels (Jercinovic et al. 2008). This process can be very time consuming for complex and chemically variable materials (e.g., monazite), but can be relatively straightforward for simple matrices such as  $SiO_2$ . Alternatively, one can perform multi-point background position measurements where multiple background positions are specified and acquired on each side of the analytical peak at the required analytical precision (Donovan 1995–2010<sup>1</sup>). Subsequently, each multi-point background intensity measurement is either selected or rejected objectively on the basis of a statistical background fit model once the data has been acquired by iteratively optimizing the fit. This alternative background fitting method will be discussed in a subsequent paper on trace element analysis.

Another difficulty exists in the choice of background fit models. For example, determination of trace Al using EPMA is sensitive to the background correction fit model used (Fig. 3).

<sup>1</sup> Donovan, J.J. (1995–2010) Probe for EPMA. <http://www.probe-software.com>. Probe Software at Microscopy & Microanalysis, Portland, Oregon.

This is especially true when the spectrometers are at low Bragg angles where the background is highly curved and/or sloped and requires the use of a more sophisticated treatment than is commonly utilized. In this example, to avoid interference from the  $\text{SiK}\alpha$  extended tailing on the low background side of the  $\text{AlK}\alpha$  peak, one might consider measuring the background only on the high side of the  $\text{AlK}\alpha$  peak. This procedure however, will greatly underestimate the background intensity underneath the analytical peak due to the highly sloping background from the  $\text{SiK}\alpha$  tailing. The more commonly utilized linear interpolation method using two background measurements on each side of the peak is an improvement but, due to the curvature of the continuum in this region of the spectrometer range, systematically reduces the net peak intensities by  $\sim 60\text{--}70$  ppm in this instance. However, using either an exponential or polynomial fit of the background, one can accurately fit both the slope and curvature of the continuum to obtain a more accurate background determination.

To properly fit a curved background with only two background intensity measurements, there are several approaches that can be utilized, but we will discuss an exponential and a polynomial fit method, where, in both cases, the user performs a spectrometer wavelength scan of sufficient precision over a

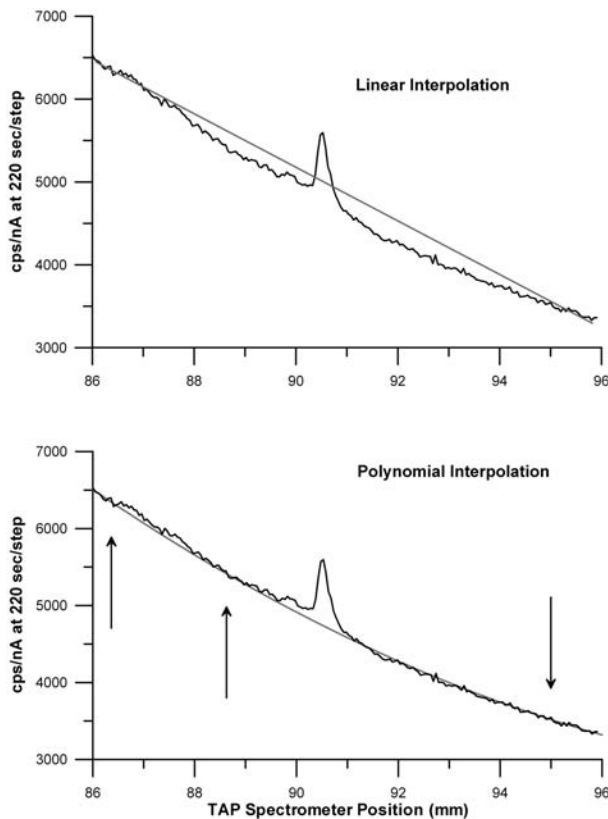


**FIGURE 3.** Wavelength intensity scan data on hydrothermal quartz in the range of the  $\text{AlK}\alpha$  peak position (black lines). The gray lines represent different background models: linear (top) and polynomial (bottom). The arrows indicate the selected fit positions for the polynomial fit regression model. The choice of background model significantly affects the apparent Al abundance.

region of interest that includes the two background measurement positions. This is the data that will be utilized to fit the selected background model, which is generally evaluated by plotting the fit model over the previously acquired spectrometer wavelength scan.

The first fit method is performed using an exponential fit expression where a user-specified “tension” parameter exponent is applied using Equation 1 until a proper fit is obtained with the wavelength scan:

$$i_{bgd} = \frac{c \cdot e^{-aP_j}}{P_j^n} \quad (1)$$

where  $c$  is a fit parameter,  $a$  is a fit parameter,  $e$  is the exponential operator,  $P_j$  is a spectrometer position, and  $n$  is a user specified exponent.

The fit parameters  $c$  and  $a$  are obtained by derivation according to the expressions shown in Equations 2 and 3.

$$c = e^{\left( \frac{[P_1 \cdot \text{Ln}(I_2) - P_2 \cdot \text{Ln}(I_1)] + n \cdot P_1 \cdot \text{Ln}(P_2) - n \cdot P_2 \cdot \text{Ln}(P_1)}{(P_1 - P_2)} \right)} \quad (2)$$

$$a = \frac{\text{Ln}(I_1) + \text{Ln}(I_2) + n \cdot [\text{Ln}(P_2) + \text{Ln}(P_1) - 2 \cdot \text{Ln}(c)]}{(P_1 + P_2)} \quad (3)$$

where  $e$  is the exponential operator,  $\text{Ln}$  is the natural log operator,  $P_1$  is the spectrometer position for the first background,  $P_2$  is the spectrometer position for the second background,  $I_1$  is the intensity measurement for the first background,  $I_2$  is the intensity measurement for the second background,  $n$  is the user specified exponent, and  $c$  is defined by Equation 2.

In this two-point exponential fit, the user-specified exponent,  $n$ , is adjusted until the fit model agrees with the wavelength intensity scan and this exponent value is stored for subsequent off-peak measurements. The on-peak position background intensity  $i_{bgd}$  is then calculated from Equation 1 after the fit parameters  $a$  and  $c$  are calculated from the two off-peak background measurements for each trace element measurement.

The polynomial background fit using two off-peak background measurements is slightly more complicated but the polynomial fit coefficients are again obtained by comparing the fit model to a previously acquired wavelength scan and storing the polynomial fit coefficients for later use with the trace element background measurements. Because the off-peak X-ray intensities may vary from one analysis to another depending on the composition of the sample (though generally not significantly for quartz because the composition is relatively constant), the polynomial regression must be normalized for the measured trace element off-peak intensities to provide a polynomial background correction for general use. Therefore, the necessary steps are as follows:

(1) Specify a polynomial fit on a previously acquired wavescan of sufficient precision using any three spectrometer positions within the scan range as shown by the arrows in Figure 3.

(2) Store the three polynomial fit regression coefficients for the element, X-ray, crystal, and spectrometer configuration and

acquire the trace element measurements using two off-peak intensity positions.

(3) Using the previously stored polynomial fit coefficients, calculate three pseudo-intensities at any three spectrometer positions (for example, the low off-peak, high off-peak, and on-peak positions from the trace element measurements). Normalize the pseudo-intensities to the same beam current as the trace element acquisition.

(4) Again, regress the three now normalized pseudo-intensities using a second-order polynomial fit.

(5) Calculate the predicted low and high off-peak intensities at the measured low and high off-peak trace element spectrometer positions.

(6) Calculate the intensity differences between the measured trace element off-peak intensities and the predicted off-peak intensities from step 5.

(7) Average the two off-peak intensity differences and add that value to the intercept coefficient from the regression fit obtained in step 4.

(8) Calculate the background intensity under the on-peak position using the modified intercept from step 7 and the slope and curvature terms obtained from the polynomial regression in step 4.

Using the above polynomial fit model in test samples measured by EPMA, the calculated Al concentrations range from 4 to 32 ppm, whereas Al values obtained by LA-ICP-MS in adjacent areas range from 2 to 33 ppm. Excellent agreement between these two techniques suggests that the exponential or polynomial background fit is appropriate for quantification of trace Al in quartz. In this particular case, any curvature of the background due to  $\text{SiK}\alpha$  extended tailing, is appropriately accounted for by measuring the background intensities on both sides of the  $\text{AlK}\alpha$  peak position and fitting an exponential or polynomial fit, because the Si content is essentially a constant for quartz samples.

### THE “BLANK” CORRECTION

Accurate trace element analyses down to a few parts per million by EPMA requires an accurate determination of the X-ray background. However, a subtle difficulty appears as EPMA detection limits are pushed below the level of several tens of parts per million. Although the precision of the EPMA can be improved by increasing beam current and/or integration time, the accuracy of the X-ray background characterization is subject to several systematic errors that cannot be eliminated by simply increasing the measurement precision. The accuracy of the background continuum determination may be affected by sample artifacts such as the matrix absorption edges, detector artifacts such as Ar or Xe absorption edges (Jercinovic and Williams 2005), and Bragg analyzing crystal diffraction artifacts such as the extended peak tails mentioned above and also “negative peaks” or “holes” in the X-ray continuum (cf. Self et al. 1990; Wark and Watson 2006). Such “negative peaks” or “holes” in the X-ray continuum, apparently due to secondary Bragg diffraction at other lattice planes at some angle to the preferred lattice plane, have been documented for the  $\text{TiK}\alpha$  X-ray peak position in quartz for some but not all PET analyzing crystals (Fig. 4). This inconsistency may be due to differences in orientation or

strain during manufacturing. Such problems in background determinations can often be avoided by simply shifting the off-peak background measurement positions, but if these artifacts are located in close proximity to the on-peak measurement position for the analytical line of interest, these systematic errors cannot be so easily avoided for the on peak intensity measurements. These X-ray continuum artifacts can produce systematic intensity errors that are measurable at levels of 20 to 50 ppm or more depending on the particular analytical situation. For example, Ti concentrations in synthetic quartz measured simultaneously on five different spectrometers—using PET and LiF crystals, range from  $-18$  to  $+24$  ppm (Table 1) with measured standard deviations on the order of 3 to 19 ppm. This demonstrates that the systematic differences between the various spectrometers, due to such continuum artifacts, can significantly exceed  $3\sigma$  sensitivities even at these relatively low precision levels obtained using moderate beam currents and counting times.

To correct for these systematic inaccuracies, a quantitative “blank” correction for EPMA has been developed that is incorporated into the traditional ZAF or  $\phi(\rho z)$  matrix correction. The term “blank” correction is appropriated from other trace element techniques such as ICP-MS, where the absolute accuracy of the measurement is characterized by analyzing a sample with a matrix similar to the unknown but, which contains none of the analyte in question (e.g., in ICP-MS pure water is generally utilized as a blank sample because pure water is generally the analyte matrix). In ICP-MS, this blank level is usually reported along with the measured values for each sample and can be subtracted

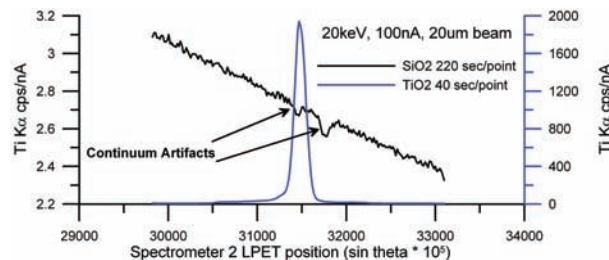


**FIGURE 4.** Wavelength dispersive scans on  $\text{SiO}_2$  and  $\text{TiO}_2$  at the position for the  $\text{TiK}\alpha$  peak showing “holes” in the continuum both adjacent to and directly underneath the analytical peak position. This scan was performed on a LPET analyzing crystal on a Cameca SX-100 EPMA instrument. Similar effects are not always observed on PET, PETJ, or PETH analyzing crystals, which may be due to different mounting orientations of the non-isometric (tetragonal) PET crystal.

**TABLE 1.** Titanium concentration values (parts per million) and measured standard deviations and standard errors on synthetic  $\text{SiO}_2$ , ESPI, Catalog K4699M (Ti confirmed at 1.42 ppm using ICP-MS) collected simultaneously on five different spectrometer-crystal combinations

Spectrometer crystal	1-PET	2-LPET	3-LPET	4-PET	5-LIF
Ti concentration average (without “blank” correction)	-3.1	-14.6	-18.0	24	1.3
Standard deviation ( $1\sigma$ )	7.5	6.9	3.6	11.7	19
Standard error ( $1\sigma$ )	2.2	2.0	1.0	3.4	5.5

Notes: Conditions were 20 keV, 100 nA, 200 s counting time for on-peak and off-peak intensities, average of 10 points. In all instances the concentration differences between spectrometers due to systematic accuracy errors are larger than the measured variances: hence, the need for an EPMA blank correction to improve absolute accuracy of trace element analysis.

from the measured values to provide a blank corrected result for best accuracy. In adopting this term for EPMA trace measurements we propose to similarly measure the analyte in question, using a zero concentration sample with a matrix similar to the actual sample (e.g., pure SiO<sub>2</sub> for the measurements reported in this paper), to obtain a characterization of the background measurement accuracy at zero concentration. However, unlike other static blank techniques, this EPMA blank concentration value is converted quantitatively into a net X-ray intensity, which is then subtracted from the measured X-ray intensity during the ZAF or  $\phi(\rho z)$  sample matrix calculation.

Applying this EPMA blank correction at somewhat more extreme beam conditions (20 keV, 200 nA, and 960 s on-peak and 960 s off-peak) as shown in Table 2, we observe that the differences between the spectrometers for two separate data sets is now similar to the precision levels for all five spectrometers, yielding ~1 to 6 ppm 1 $\sigma$  variances. This compares well to predicted 3 $\sigma$  variances calculated by assuming only random counting statistics that gives ~4 to 7 ppm using Equation 4. Alternatively, 3 $\sigma$  detection limits derived from Scott and Love (1983), which also include sample matrix effects, range from 5 to 8 ppm, again providing good agreement with theoretically achievable sensitivities:

$$X_U = \frac{3\sqrt{I_U^B \cdot t_U^B \cdot B_U \cdot C_S}}{I_U^B \cdot B_U \cdot I_S^P} \quad (4)$$

where  $I_U^B$  is the intensity of the background in cps/nA,  $t_U^B$  is the count time used for the unknown background measurement,  $B_U$  is the beam current used for the unknown measurement in nA,  $C_S$  is the concentration of the element in the standard in weight percent,  $I_S^P$  is the intensity of the standard in cps/nA, and  $X_U$  is the detection limit concentration in weight percent.

**TABLE 2.** TiK $\alpha$  EPMA element statistics (parts per million) on two measurement sets of synthetic SiO<sub>2</sub>, ESPI, Catalog K4699M (Ti confirmed at 1.42 ppm using ICP-MS)

Spectrometer crystal	1-PET	2-LPET	3-LPET	4-PET	4-PET
Set 1, Ti concentration average (without blank correction)	-0.8	-12.3	-29.5	4.7	-3.4
Set 2, Ti concentration average (without blank correction)	1.2	-11.4	-29.7	7.3	-1.4
Set 1, Ti concentration average (with blank correction)	-0.6	0.5	1.6	-1.2	-0.6
Set 2, Ti concentration average (with blank correction)	3.5	2.3	1.2	4.0	3.4
Set 1, measured dev. (1 $\sigma$ )	5.8	2.3	1.2	6.5	2.3
Set 2, measured dev. (1 $\sigma$ )	3.9	2.7	3.5	5.2	1.4
Set 1, predicted detection (3 $\sigma$ )	6.1	4.2	4.0	6.9	5.8
Set 2, predicted detection (3 $\sigma$ )	6.1	4.2	4.0	6.9	5.8
Set 1, reported detection (3 $\sigma$ )	7.2	4.9	4.7	8.0	6.8
Set 2, reported detection (3 $\sigma$ )	7.2	4.9	4.7	8.0	6.8
Set 1, detection 95% CI t-test (avg.)	5.8	1.8	3.1	5.6	3.2
Set 2, detection 95% CI t-test (avg.)	6.5	3.0	4.7	1.4	5.1
Set 1, detection 99% CI t-test (avg.)	9.5	2.9	5.1	9.2	5.3
Set 2, detection 99% CI t-test (avg.)	10.7	5.0	7.8	2.2	8.4

Notes: Testing with and without using blank corrected intensities, on 5 spectrometers acquired at 20 keV, 200 nA beam current and 960 s on peak and 960 s off peak, average of 5 points. The blank corrected Ti concentrations are only provided to demonstrate the improvement in spectrometer-to-spectrometer variation because they are referencing each other for the purposes of a blank correction in this study. The "predicted" detection limit is based on the 3 $\sigma$  estimate of the measured background variance from Equation 4. The "reported" detection includes the additional effect of the sample matrix correction (cf. Scott and Love 1983), which for TiK $\alpha$  in SiO<sub>2</sub> relative to TiO<sub>2</sub> is about 1.2, mostly due to the atomic number effect.

Additional sensitivity calculations utilizing a t-test for the average of 5 data points in two separate data sets yields ~2 to 7 ppm at 95% confidence intervals (CI) and 3 to 10 ppm at 99% CI for individual spectrometers.

Thus, the EPMA blank correction provides a quantitative accuracy correction to the net X-ray intensities, by calculating the intensity contribution from the measured systematic quantitative offset as shown in Equation 5, from a trace calibration standard, which is measured under identical conditions as the unknown sample. Note that the calibration level in the blank standard,  $C_{level}$ , need not be zero; it can be any known non-zero trace level for the purposes of this correction. And because the calibration intensity from the blank standard is quantitatively corrected for both continuum background and compositional matrix effects relative to the unknown in question, the matrix of the blank calibration standard need not be identical to the unknown matrix. However, because there are at least two sources of systematic errors that can be corrected for using the blank correction, it is worth noting that the selection of a blank calibration standard with an appropriate matrix is important in some cases. For example, the matrix of the blank calibration standard is critical when correcting for a matrix induced continuum artifact, such as the measurement of AlK $\alpha$  in a SiO<sub>2</sub> matrix as described above. In this case, the shape of the background is strongly affected by the tail of the SiK $\alpha$  peak and therefore requires a blank standard with a similar SiO<sub>2</sub> matrix. On the other hand, for instrumental sources of systematic error, such as the "negative peaks" or "holes" in the TiK $\alpha$  background resulting from secondary Bragg diffraction on some PET crystals, the blank calibration standard does not need to be similar in matrix to the unknown. In this instance, the blank calibration standard needs only to be well-characterized compositionally for the trace element being measured in the unknown because the source of systematic accuracy error is due to instrumentally induced differences between the WDS spectrometers.

This EPMA blank correction is applied iteratively using Equation 5 during the sample matrix correction iteration so that the elemental k-ratios (i.e., the unknown net intensities divided by standard net intensities), peak-to-backgrounds (P/B) and other error calculations are properly propagated.

$$I_{corr} = I_{unk} - I_{std} \frac{(C_{meas} - C_{level}) [ZAF]_{std}}{C_{std} [ZAF]_{unk}} \quad (5)$$

where  $I_{corr}$  is the blank corrected unknown net intensity,  $I_{unk}$  is the measured unknown net intensity,  $I_{std}$  is the measured primary standard net intensity,  $C_{meas}$  is the measured concentration in the blank standard,  $C_{level}$  is the zero or known concentration in the blank standard,  $C_{std}$  is the concentration in the primary standard (TiO<sub>2</sub>),  $ZAF_{std}$  is the matrix correction factor for the primary standard (TiO<sub>2</sub>),  $ZAF_{unk}$  is the matrix correction factor for the unknown sample.

Results obtained using this new matrix-iterated trace element EPMA blank correction method demonstrate that these systematic errors can be reduced to levels similar to the measured detection limits that can be as low as single digit parts per million values when combined with the "aggregate" intensity method described below. The Ti concentrations in parts per million between two different spectrometers obtained from a stage line scan analysis

across a hydrothermal quartz vein sample are shown in Figure 5. Although the average Ti concentration in this sample is on the order of 300 ppm, the difference between the corrected and un-corrected “blank” results from the two spectrometers is ~40 ppm or more than a 10% relative error due to differences in the continuum artifacts intrinsic to each spectrometer. Note that at sub-100 ppm levels, this ~40 ppm discrepancy would be similar in magnitude to the measured concentrations. The applied EPMA blank correction quantitatively minimizes this systematic concentration offset to levels similar to the measured precision.

#### AGGREGATE INTENSITY COUNTING

Although accuracy can be improved through careful use of the blank correction procedure described above, precision is still often a limiting factor for EPMA trace element measurements. There are, of course, several prosaic approaches to increase the characteristic X-ray signal including: increased accelerating voltage, increased beam current, or increased count integration time or a combination of these approaches. Increased accelerating voltage and beam current can result in greater precision by increasing the ionization efficiency and electron flux, but this also results in larger interaction volumes and possible increased sample damage. Increased count time improves statistics simply by increasing the total number of photons integrated at the cost of increased analysis time and possible increased sample damage and/or charging. Many analysts are familiar with the appearance of small areas of visual damage produced by a focused electron beam in quartz samples after an extended period of electron beam exposure. This beam damage effect, although significantly less observable in specimens of SiO<sub>2</sub> glass under the same beam conditions and exposure times, is quite noticeable in crystalline SiO<sub>2</sub> (Hobbs and Pascucci 1980), and therefore limits these simple approaches for improving sensitivity in quartz. Previous X-ray intensity measurements performed to characterize the time dependence of such effects show that significant changes in SiK $\alpha$  intensities occur after ~5 to 10 min of even moderate (30 to 50 nA) beam exposure with a focused beam. Emitted intensities

of OK $\alpha$  in SiO<sub>2</sub> are affected by such moderate electron beam exposures in even less time (Donovan and Rowe 2005).

Another approach to improving trace element detection limits is to increase the geometric efficiency of the instrument by various engineered strategies including decreasing the Rowland focal circle, using larger Bragg analyzing crystals or combining X-ray intensities from multiple spectrometers. Smaller focal circles will improve geometric efficiency and produce significantly higher X-ray intensities at a given beam current, but they also result in lower spectral resolution. Large area Bragg crystals are an excellent approach for improving geometric efficiency of the instrument but the availability of this method is usually fixed at the time of the instrument purchase and, in any case, adds considerable cost to the instrument purchase or upgrade. In all cases however, one can improve the geometric efficiency of the EPMA instrument by utilizing software to combine the photon streams from two or more Bragg spectrometers tuned for the same element emission line, although the Bragg crystals may be of different types (e.g., LiF and PET).

The combining of photon intensities from multiple spectrometers, as opposed to the calculated concentrations, has the advantage that all counting statistics are then automatically propagated (and properly weighted) in all subsequent calculations. To ensure quantitative accuracy, the combining of intensities at the photon intensity must be applied to both the acquisition of the unknown and the standard intensities. Although each spectrometer contributes photon counts at rates specific to its own individual design, construction, configuration, and tuning, all photon count rates can be combined in software to yield a count rate equivalent to a single spectrometer with greater geometric efficiency, assuming that each spectrometer is tuned to the same element and emission line, and the intensities are separately corrected for deadtime (and beam drift) before they are combined in software. Note that the on peak, high off-peak and low off-peak intensities (and multi-point background intensities if utilized) must also be aggregated separately using deadtime corrected photon intensity levels so that detection limit statistics can be properly propagated during

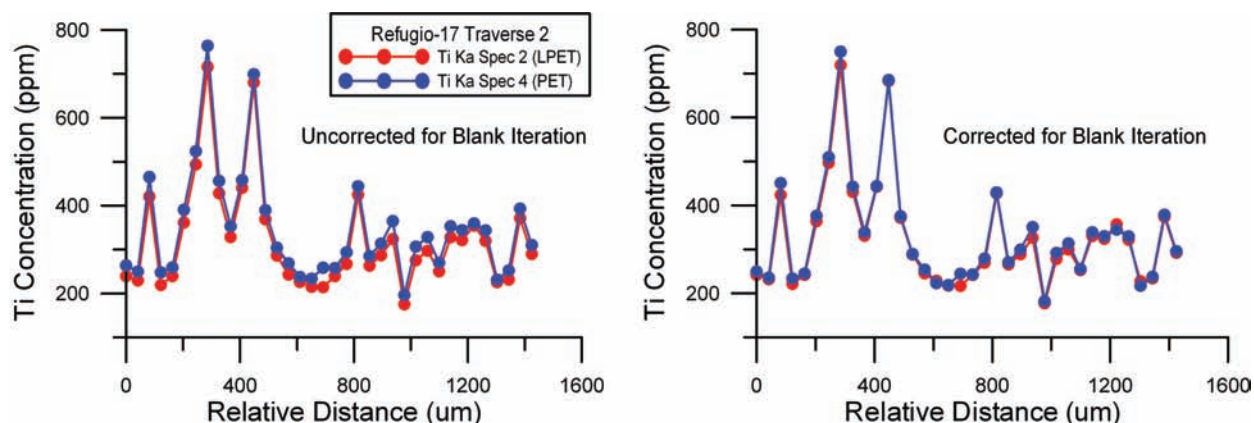


FIGURE 5. Quantitative Ti linescan from a Cameca SX-100 EPMA across a hydrothermal quartz vein shows that, even at relatively high concentrations of several hundred parts per million, systematic differences between two spectrometers due to instrument/spectrometer/crystal-dependent continuum artifacts are distinctly visible. Data values over 400 ppm were adjacent to rutile inclusions in the quartz vein. Differences between the two spectrometers are ~40 ppm at the 300 ppm level before the application of the blank correction (left). After the blank correction (right) is performed, the systematic differences between the two spectrometers are significantly smaller and within the precision levels.

subsequent calculations.

The analytical approach wherein the same element is simultaneously acquired on multiple spectrometers and combined by software at the photon intensity level is referred to as “aggregate” intensity counting. In aggregate intensity counting, both the on- and the off-peak intensities of the duplicate elements are aggregated to improve the total counting statistics. This does not physically measure more of a specific element in the sample because the standard intensities are also measured and aggregated under the same spectrometer configuration (though not necessarily the same beam or count time) conditions. However, if the same element is measured on multiple spectrometers and not combined as aggregate intensities, the duplicate concentrations will be added to the sample matrix correction and this could result in systematic errors to the matrix correction, especially if the duplicate element is present at significantly more than trace level concentrations. In any case, it is useful to switch the software between aggregate and non-aggregate intensity modes with the same data set, to evaluate the relative performance of individual spectrometers for detection limit comparisons. It should be noted that aggregate cps/nA intensities that require de-normalizing to time and beam current for proper statistical calculations must be de-normalized to both the average counting time and the average beam current for situations in which different count times or beam currents were utilized for duplicate element measurements. For best analytical results, the individual spectrometer intensities should always be blank corrected prior to using the aggregate intensity method to avoid decreased precision from combining systematic net intensity offsets between spectrometers.

A summary of measurement statistics from all 5 spectrometers tuned to  $TiK\alpha$  and measured on pure  $SiO_2$  (1.42 ppm Ti by ICP-MS) calculated with the aggregate intensity correction option is shown in Table 3. Three  $\sigma$  sensitivities based on counting statistics only are  $\sim 2.5$  ppm, while t-test sensitivities on the average of 5 data points yields  $\sim 1.5$  to 2 ppm at 95% CI and  $\sim 2.5$  to 3 ppm at 99% CI, all of which demonstrate the efficacy of the aggregate intensity method particularly when utilized with the blank correction.

### TEST OF METHODOLOGY

To further test the accuracy and precision of EPMA analyses using the methods described in this paper, a synthetic quartz standard (ESPI, Catalog K4699M) was analyzed by ICP-MS

**TABLE 3.**  $TiK\alpha$  EPMA element statistics (parts per million) on two data sets of synthetic  $SiO_2$ , ESPI, Catalog K4699M (Ti confirmed at 1.42 ppm using ICP-MS)

5 spectrometers (all PET crystals)	With aggregate intensity option
Set 1, Ti concentration average	0.5
Set 2, Ti concentration average	2.4
Set 1, reported detection ( $3\sigma$ )	2.5
Set 2, reported detection ( $3\sigma$ )	2.5
Set 1, detection 95% CI t-test (avg.)	1.5
Set 2, detection 95% CI t-test (avg.)	1.9
Set 1, detection 99% CI t-test (avg.)	2.5
Set 2, detection 99% CI t-test (avg.)	3.1

*Notes:* Testing done on 5 spectrometers (20 keV, 200 nA beam current, and 960 s on-peak and 960 s off-peak, average of 5 points), using blank corrected intensities along with the aggregate intensity option that combines photon intensities from all duplicate element spectrometers to improve geometric efficiency by approximately a factor of five and therefore sensitivity levels by approximately a factor of 2 to 3.

following the procedure in Taggart (2002) and found to have  $<2$  ppm Ti, Al, and Zn and 3 ppm Li and Mn. All other elements were present at the  $<1$  ppm level. EPMA data were collected at the University of Oregon using a Cameca SX-100 with Probe for EPMA software (cf. Donovan 1995–2010<sup>1</sup>). The operating conditions were 20 keV, 200 nA and utilized several increasing count integration times between 2 and 1920 s for both the on-peak and off-peak intensities for the test measurements, using PET or LPET crystals on all 5 spectrometers. The on-peak and off-peak intensities for all measurements over 60 s in duration were acquired using alternating on-peak and off-peak intervals to compensate for any change in intensity over time. For example, the 960 second on-peak counting interval consisted of 16 separate 60 second on-peak measurements, with 30 s of high off-peak measurement followed by 30 s of low off-peak measurement interleaved between the on-peak intensity measurements.

A summary of the calculated single point detection limits and t-test detection limits for the average of 5 points comparing single spectrometer statistics and the aggregate intensity method are shown in Figures 6 and 7. Detection limits in Figure 6 were calculated using the method of Scott and Love (1983), which assumes detection at 3 times the variance of the background determination plus an adjustment for matrix effects. The t-test detection limits in Figure 7 were calculated from Goldstein et al. (1992). Note that the aggregate intensity method produces a 60% CI detection limit significantly below that of the single spectrometer 60% CI.

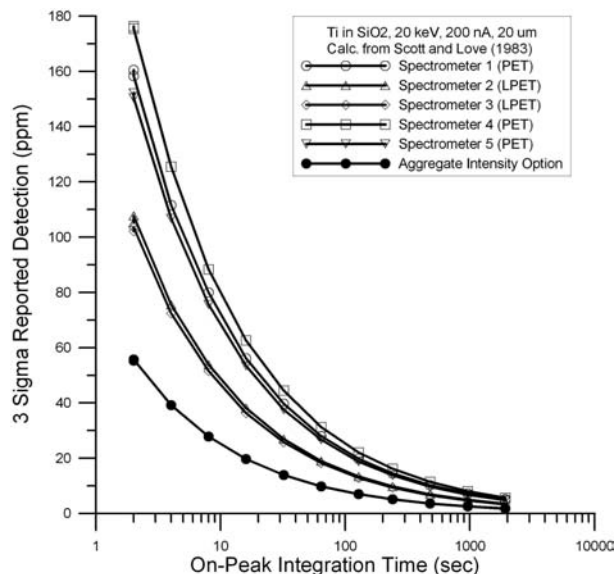


**FIGURE 6.** Comparison of individual spectrometer  $3\sigma$  detection limits with the software-enabled “aggregate” intensity option as a function of counting time as measured on a pure  $SiO_2$  “blank” (1.42 ppm Ti by ICP-MS). The aggregate intensity option reflects the combined intensities of all 5 individual spectrometers. Data was acquired on a Cameca SX-100 with 5 spectrometers using PET and LPET crystals. Note that the large area crystals produce the lowest detection limits for an individual spectrometer, but the aggregate intensity option curve consisting of the combined intensities from all 5 spectrometers greatly outperforms any individual spectrometer’s performance.

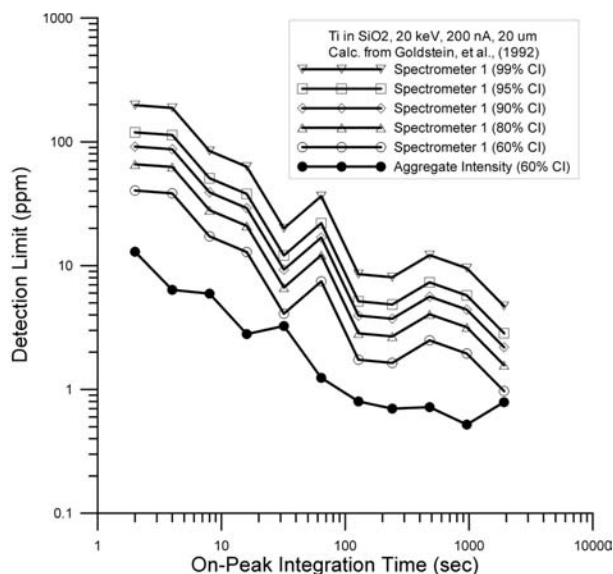


**FIGURE 7.** Comparison of individual spectrometer detection limit t-tests, 60 to 99% confidence intervals (CI), along with the software enabled aggregate intensity option at 60% CI as a function of counting time as measured on pure  $\text{SiO}_2$  (1.42 ppm Ti by ICP-MS). The t-test detection limits were calculated using the method of Goldstein et al. (1992). Data was acquired on a Cameca SX-100 with 5 spectrometers. For counting times exceeding 100 s, the 60% CI t-test for the blank corrected and aggregate intensities were at or below the 1 ppm level.

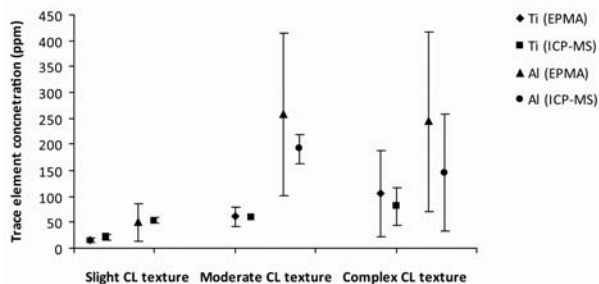


**FIGURE 8.** Average Al and Ti concentrations of 3 samples of hydrothermal vein quartz analyzed by LA-ICP-MS and a JEOL 8900 EPMA. Each point represents the average of between 5 and 20 analyses. Error bars represent 1 st.dev. Electron microprobe analyses have wider standard deviations than LA-ICP-MS, because of the higher spatial resolution of EPMA, in quartz with a wide range of CL intensities. In samples with complex CL textures, the effect of resolution is emphasized for the smaller EPMA analysis areas, as LA-ICP-MS spot analyses included more than one generation of quartz so that high and low values are less likely.

In addition, several samples of hydrothermal quartz crystals were characterized by SEM-CL and then analyzed by EPMA and LA-ICP-MS at the U.S. Geological Survey in Denver. EPMA data were acquired using a JEOL 8900 with Probe for EPMA software (cf. Donovan 1995–2010<sup>1</sup>). Operating conditions were 20 kV, 100 nA, using a spot or 5  $\mu\text{m}$  defocused beam. Peak and background counting times were acquired for 600 s each. On- and off-peak intensities were acquired repeatedly for each data point to account for sample degradation and carbon contamination

buildup from beam heating. The blank correction and aggregate intensity option described in this paper were applied to the Ti and Al measurements and EPMA results obtained on these quartz veins is in excellent agreement with LA-ICP-MS analyses of the same sample (Fig. 8).

EPMA analysis of Ti and Al in quartz at the <10 ppm level can now be achieved using a combination of blank correction, aggregate intensity software options, and careful attention to the use of exponential or polynomial background fit models. By utilizing all these methods simultaneously, one can combine net intensities from multiple spectrometers with systematic errors similar to the measured sensitivities. These techniques result in excellent precision and accuracy at levels well below 10 ppm. These new trace detection limits allow EPMA analytical resolution on the same spatial order as CL features to decipher the chemical and physical history of quartz crystallization in a range of geologic environments.

## ACKNOWLEDGMENTS

The authors acknowledge Paul Carpenter, John Fournelle, and Dale Newbury for their excellent comments on this manuscript, and thanks to Celeste Mercer for work on Figure 2. Alan Koenig, Paul Lamothe, Ruth Wolf, and Monique Adams of the U.S. Geological Survey for their ICP-MS data on the quartz standard. Brian Rusk acknowledges the USGS Mendenhall Fellowship.

## REFERENCES CITED

- Allan, M.M. and Yardley, B.W.D. (2007) Tracking meteoric water infiltration into a magmatic hydrothermal system: A cathodoluminescence, oxygen isotope, and trace element study of quartz from Mt. Leyshon, Australia. *Chemical Geology*, 240, 343–360.
- Donovan, J.J., Snyder, A., and Rivers, M.L. (1993) An improved interference correction for trace element analysis. *Microbeam Analysis*, 2, 23–28.
- Donovan, J.J. and Rowe, M. (2005) Techniques for improving quantitative analysis of mineral glasses. *Geochimica et Cosmochimica Acta Supplement*, 69, 10, Supplement 1, Goldschmidt Conference Abstracts, A589
- Escuder, J.A., Salvat, F., Llovet, X., and Donovan, J.J. (2010) Numerical Correction for secondary fluorescence across phase boundaries in EPMA, 11th European Workshop on Modern Developments and Applications in Microbeam Analysis IOP Publishing IOP Conf. Series. Materials Science and Engineering, 7, 012008.
- Goldstein, J.I., Newbury, D.E., Echlin, P., Joy, D.C., Lyman, C.E., Lifshin, E., Sawyer, L.C., and Michael, J.R. (1992) *Scanning electron microscopy and X-ray microanalysis: A text for biologists, materials scientists, and geologists* (2<sup>nd</sup> ed.), p. 436. Plenum Press, New York.
- Hobbs, L.W. and Pascucci, M.R. (1980) Radiolysis and defect structure in electron-irradiated  $\alpha$ -quartz. *Journal de Physique*, 7, Tome 41, Juillet C6-237.
- Jercinovic, M.J. and Williams, M.L. (2005) Analytical perils (and progress) in electron probe microanalysis trace element analysis applied to geochronology: Background acquisition, interferences, and beam irradiation effects. *American Mineralogist*, 90, 526–546.
- Jercinovic, M.J., Williams, M.L., and Lane, E.D. (2008) In-situ trace element analysis of monazite and other fine-grained accessory minerals by EPMA. *Chemical Geology*, 254, 3–4, 197–215
- Landtwing, M. and Pettke, T. (2005) Relationships between SEM-cathodoluminescence response and trace element composition of hydrothermal vein quartz. *American Mineralogist*, 90, 122–131.
- Larsen, R.B., Jacamon, F., and Krantz, A. (2009) Trace element chemistry and textures of quartz during the magmatic-hydrothermal transition of Oslo Rift granites. *Mineralogical Magazine*, 73, 691–707.
- Lehmann, K., Berger, A., Gotte, T., Ramseier, K., and Wiedenbeck, M. (2009) Growth related zonation in authigenic and hydrothermal quartz characterized by SIMS, EPMA, SEM-CL, and SEM-CC-imaging. *Mineralogical Magazine*, 73, 633–643.
- Llovet, X. and Galan, G. (2003) Correction of secondary X-ray fluorescence near grain boundaries in electron microprobe analysis: Application to thermobarometry of spinel hercynites. *American Mineralogist*, 88, 121–130.
- Mercer, C.N. and Reed, M.H. (2010) The temperature connection between magmatic and hydrothermal realms of the porphyry-Cu-Mo deposit at Butte, Montana. *Economic Geology*, in press.
- Monecke, T., Kempe, U., and Götz, J. (2002) Genetic significance of the trace element content in metamorphic and hydrothermal quartz: A reconnaissance study. *Earth and Planetary Science Letters*, 202, 709–724.

- Müller, A. and Koch-Muller, M. (2009) Hydrogen speciation and trace element contents of igneous, hydrothermal and metamorphic quartz from Norway. *Mineralogical Magazine*, 73, 569–583.
- Penniston-Dorland, S.C. (2001) Illumination of vein quartz textures in a porphyry copper ore deposit using scanned cathodoluminescence: Grasberg Igneous Complex, Irian Jaya, Indonesia. *American Mineralogist*, 86, 652–666.
- Rusk, B. and Reed, M. (2002) Scanning electron microscope-cathodoluminescence analysis of quartz reveals complex growth histories in veins from the Butte porphyry copper deposit, Montana. *Geology*, 30, 727–730.
- Rusk, B., Reed, M., Dilles, J., and Kent, A. (2006) Intensity of quartz cathodoluminescence and trace element content of quartz from the porphyry copper deposit in Butte, Montana. *American Mineralogist*, 91, 1300–1312.
- Rusk, B.G., Lowers, H.A., and Reed, M.H. (2008) Trace elements in hydrothermal quartz: Relationships to cathodoluminescent textures and insights into vein formation. *Geology*, 36, 547–550.
- Scott, V.D. and Love, G. (1983) *Quantitative electron-probe microanalysis*. Wiley, New York.
- Self, P.G., Norrish, K., Milnes, A.R., Graham, J., and Robinson, B.W. (1990) Holes in the background in XRS. *X-ray Spectrometry*, 19, 59–61.
- Taggart, J.E. (2002) Analytical methods for chemical analysis of geologic and other materials. U.S. Geological Survey Open-File Report, 02-223-V.
- Thomas, B.T., Watson, E.B., Spear, F.S., Shemella, P.T., Nayak, S.K., and Lanzarotti, A. (2010) TitaniQ under pressure: The effect of pressure and temperature on the solubility of Ti in quartz. *Contributions to Mineralogy and Petrology*, 160, 743–759, DOI: 10.1007/s00410-010-0505-3.
- Wark, D.A. and Watson, B.E. (2006) TitaniQ: A titanium in quartz geothermometer. *Contributions to Mineralogy and Petrology*, 152, 743–754.
- Wark, D.A., Hildreth, W., Spear, F.S., Cherniak, D.J., and Watson, E.B. (2007) Pre-eruptive recharge of the Bishop magma system. *Geology*, 35, 235–238.

MANUSCRIPT RECEIVED JUNE 14, 2010

MANUSCRIPT ACCEPTED OCTOBER 1, 2010

MANUSCRIPT HANDLED BY VIRGINIA PETERSON